Heat Flux Evaluation Methods for a Single Element Heat-Sink Chamber

M. P. Celano[⋆] [†], *S. Silvestri*[⋆], *J. Pauw*[⋆], *N. Perakis*[⋆], *F. Schily*[⋆],
D. Suslov[⋆⋆] *and O J. Haidn*[⋆]
[⋆]*Institute for Flight Propulsion (LFA), Technische Universität München (TUM), Germany*
[⋆⋆]*German Aerospace Center (DLR), Lampoldshausen, Germany*
[†] Corresponding Author

Abstract

The presented study aims to contribute to the understanding of the thermal transfer and mixing processes for the new propellant combination GOX/GCH_4. A single element shear coaxial injector combustion chamber is operated at conditions typical for rocket engines,to provide a benchmark for the validation of combustion modelling codes. To investigate the heat transfer characteristics different methods, which make use of a series of wall temperature measurements, are presented. An FE as well as an FD analysis, both for a 2D and for a 3D model, are developed. The key parameters and calculation techniques are introduced. Experimental data, obtained with the heat-sink single element combustion chamber at a pressure of 2 MPa and a mixture ratio of 2.2 (*CASE A*) and 3.4 (*CASE B*), are used to validate the codes. Results obtained from the different calculation methods are analyzed and compared. A good agreement is shown for all evaluated load points.

Nomenclature

A	:	cross sectional area (m^2)	λ	:	heat conduction (W/mK)
a	:	thermal diffusivity (J/m^3K)	δ	:	Dirac operator
c	:	specific heat capacity (J/kgK)	ρ	:	density (kg/m^3)
E	:	energy (J)	θ	:	temperature variation
FD	:	Finite Difference	Subscripts		
FE	:	Finite Element	0	:	initial time
GOX	:	gaseous oxygen	cc	:	combustion chamber
GCH_4	:	gaseous methane	end	:	ending condition
g	:	Lagrange multipliers	$eval$	:	evaluation condition
I	:	impulse ratio methane/oxygen	in	:	entry condition
J	:	residual function	M	:	measurement
L	:	Lagrange function	out	:	exit condition
m	:	mass (kg)	$start$	:	starting condition
$\dot{m}$	:	mass flow rate (kg/s)	$stor$	:	storage
n	:	exponent for heat flux correlation	th	:	throat
P	:	pressure (MPa)	w	:	wall
$\dot{q}$	:	heat flux (W/m^2)			
r	:	radius of the control volume (m)			
T	:	temperature (K)			
t	:	time (s)			
ROF	:	mixture ratio of oxidizer/fuel			
S	:	Jacobi matrix			
VR	:	velocity ratio methane/oxygen			
X	:	shape factor (m)			
x	:	coord. orthogonal to hot gas direction (m)			
y	:	coord. orthogonal to hot gas direction (m)			
z	:	coord. along chamber axis (m)			

Copyright © 2015 by [Celano et al.]. Published by the EUCASS association with permission.

1. Introduction

Over the past decades, considerable effort has been dedicated to model combustion in rocket chambers in order to understand and predict the conjugate heat transfer to the chamber walls. Validations of computational fluid dynamics design tools require, in turn, reliable experimental data assessment. This involves the need to acquire a comprehensive set of data in the same facility, including wall heat fluxes along with inflow measurements over a broad range of operational conditions. Such a constraint becomes even more critical in case of innovative propellant combinations like methane and oxygen, where not well-validated combustion and heat transfer models exist. Although this propellant combination is an attractive option, only a limited amount of experimental data is available at relevant combustion chamber conditions[1,2] and a critical gap is present in the knowledge of detailed heat transfer characteristics and injector technology. When developing an engine and the correlated injection system, there are the key factors that must be considered: the heat transfer characteristic, the combustion efficiency and the combustion stability. While the combustion efficiency and combustion stability can be easily obtained by measuring the chamber pressure, it is always quite challenging, to get a detailed information on the temperature and the heat loads at the chamber walls due to the extremly harsh environment. The heat flux distribution plays definetively an important role and it has a great impact on the complete engine. Therefore, its detailed knowledge is mandatory. The strength, the life-cycle, the cooling system effectiveness as the engine-cycle are stricly connected to the heat loads experienced in the combustion chamber.

The current study aims to enlarge the available data base for methane-oxygen combustion and to provide efficient tools to analyse the hot gas wall conditions. With this purpose, a heat-sink single element combustion chamber is tested over a wide range of combustion pressures and mixture ratios. However it has to be taken into account that, the measurement of transient heat fluxes and temperatures in a heat-sink combustion chamber continues to present technical challenges in the field of instrumentation engineering. Sensor failure rates are high, and the measurement accurancies as well as measurement uncertainities are no well characterized. Even though a numerous types of heat flux sensors is present on the market, only a small subset is capable to operate in rocket combustion chambers. Furthermore in heat-sink chambers it is quite common to find that for those sensors the junction disappears at some point during a test, and the sensor fails. Other methods have been developed which do not rely on surface temperature measurements but on embeded sensors within the walls.[3] The sensors are in this way protected from erosion phenomena. In the context of this work, the second solution has been adopted. A set of 29 thermocouples is installed with a regular pattern in the combustion chamber walls. Once the sensor signals are acquired, models of different complexity are used to reduce the transient temperatures to the heat load, which the chamber walls are subject to, by numerically solving the heat conduction equation. The results obtained by different approaches are validated and the error generated by neglecting secondary phenomena, like transversal heat or by reducing the complexity of the system to a 1-D unsteady heat conduction model, is estimated. Code outcomes for the GOX/GCH4 single-element shear coaxial injector at nominal combustion pressure of 2 MPa for two operating conditions are shown. The load points are chosen such that the VR and I, characteristic numbers for the shear mixing, have their maximum range of variation for the present injector design in gas-gas conditions, taking into account the flammability limits of methane and the safe operation of the combustion chamber. Such kind of variation aims to show the sensitivity of the developed tools to change in operating conditions.

2. Hardware set-up and operating conditions

In this section a description of the instrumented single element rocket chamber, the injector geometry, and the flow conditions used for the wall heat flux characterization, are presented. The test campaign is performed using a modular heat-sink combustion chamber with an inner square cross section, designed for a testing time of up to 4 s at a chamber pressure of 2 MPa and mixture ratio of 3.4. The single-element rocket combustion chamber is depicted in Fig. 1. The inner chamber dimensions are shown in Table 1.

In recent years Pennsylvania State University, University of Florida, NASA MSFC and Beijing University of Aeronautic and Astronautic made many attempts[4–7] on studying heat transfer in heat sink chambers. A heat sink chamber design is in fact preferable in the initial phase of a research project because of its simplicity, low structural costs, ease to manufacture and high accessibility for thermocouple installation.

Table 1: Combustion chamber dimensions

Chamber length	[m]	0.290
Chamber width	[m]	0.012
Chamber height	[m]	0.012
Throat height	[m]	0.0048
Contraction ratio A_{cc}/A_{th}	[-]	2.5

For the current study, a single shear coaxial injector element is integrated as shown in Fig. 1 with a 4 *mm* diameter for

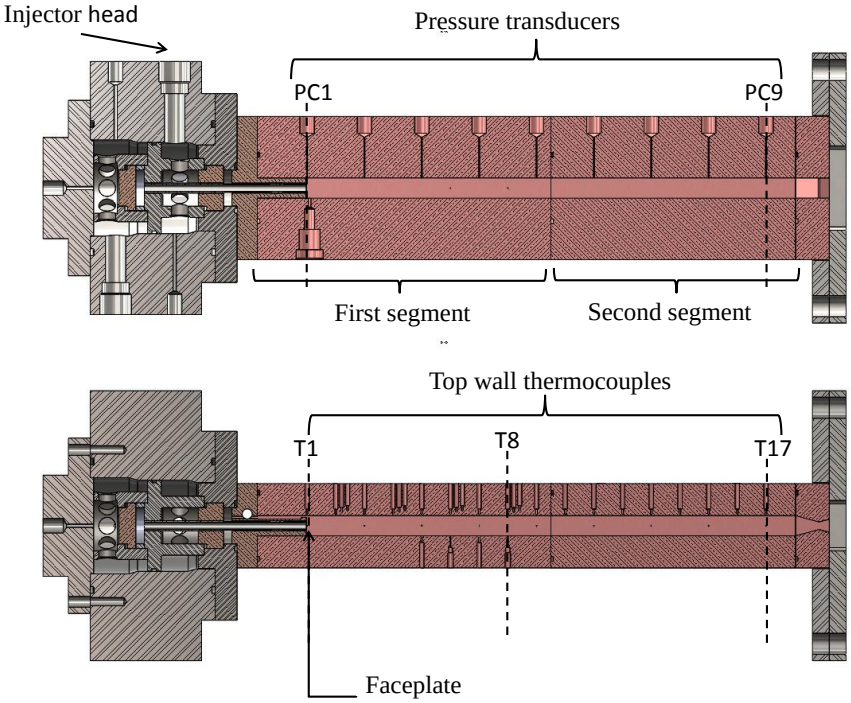

Figure 1: Horizontal (up) and vertical (down) cross section of the heat-sink combustion chamber

the central oxygen jet and a 0.5 *mm* annular gap for the methane flow. For simplicity, the GOX post is configured flush with respect to the injection face (no recess). The material used for the chamber segments and the nozzle segment is oxygen-free copper (Cu-HCP).

The presented methods for heat flux evaluation rely on thermocouple measurements at a series of points near the combustion chamber walls. Therefore, a series of Type T 0.5 *mm* diameter thermocouples is embedded at equaly spaced positions along the axial direction in the heat-sink chamber. The distance of these points to the internal surface is kept constant and equal to 1 *mm*. The longitudinal locations of the heat flux thermocouples are referred to as T1..T17. Along the chamber wall a regular pitch of 17 *mm* between two measurement positions is kept , with the injector face taken as the reference plane. With the development of the combustion flow in the chamber, a heat flux profile is generated on the inner wall in flow direction, which further results in a temperature profile on the measurement points. Therefore, the temperature readings can be employed to determine the heat flux on the combustion chamber wall.

Together with temperature measurements, the hardware allows for a detailed determination of the pressure decay along the combustion chamber wall via a series of pressure transducers ($PC1$ to $PC9$) installed in the side walls with a constant pitch of 34 *mm*. More details about the experimental set-up can be found in previous publications.[8]

The use of a heat sink hardware limits the duration of every firing test, thus the burn time is chosen equal to 3 *s* to reach stable operation of the combustion chamber, required for the thermal load measurements. Each of the operating points is run at least two times to ensure the repeatability of the recorded test data. Good agreement is obtained for all load points. In the light of the fact that the igniter mass flow rate is less than 1 g/s and that the total operating time of the igniter is less than 0.3 *s*, the influence of the ignition on the wall temperature is in the present study neglected. As an example of the test results obtained in the current test campaign, in the following section the 2 MPa $ROF = 2.2$ ($CASE\ A$) and 2 MPa, $ROF = 3.4$ ($CASE\ B$) test cases are shown in more details, see Table 2. These two

Table 2: Operating conditions

Case	ROF	$\dot{m}$		T		I	VR
	Ratio	GOX	GCH4	GOX	GCH4		
	$[-]$	$[g/s]$	$[g/s]$	$[K]$	$[K]$	$[-]$	$[-]$
A	2.20	44.2	20.1	280.7	275.9	0.74	1.2
B	3.45	46.5	13.4	281.7	280.5	0.39	0.89

load points are choseen such to represent the two extremes for the mixing process for the installed injector. In a coaxial injector the shear forces between the propellants establish the mixing efficiency. Non-dimensional numbers such as the velocity ratio VR (Eq. 1) and the momentum flux ratio I (Eq. 2) are employed to characterize injection conditions.

$$VR = \frac{v_{\mathrm{GCH4}}}{v_{\mathrm{GOX}}} \quad (1) \qquad I = \frac{(\rho v^2)_{\mathrm{GCH4}}}{(\rho v^2)_{\mathrm{GOX}}} \quad (2)$$

The variation of these values influences the form and the structure of the flame. Therefore, differences have to be expected in the shape of the heat flux profile. Furthermore it has to be noted that, for the two cases considered, the VR once is bigger than one and once is smaller than one, which means that in *CASE A* the methane jet is faster the one of oxygen, whereas in *CASE B* the oxygen jet is the faster.

3. Heat Flux Calculations

The characteristic of an injector element is mainly defined by the heat flux distribution on the hot wall along the chamber axis. The mixing mechanisms in the near injector field determine the flow conditions and influence flame and flow dynamics as well as its performance. The axial (z-axis) and perpendicular (x-axis) distribution of the thermocouples allows the determination of the heat flux variation along the axis and the reconstruction of the thermal field in the chamber wall. In the present paragraph the distributions of the temperature and heat flux on the inner chamber walls and their transient behavior during the hot run are shown. The temperature evolution over time in Fig. 2 shows that no steady state conditions are reached in the chamber during the hot run.

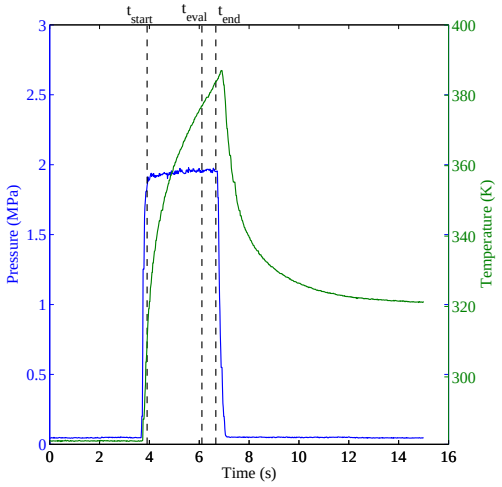

Figure 2: Typical temperature and pressure evolution during an hot run

A time-dependent temperature field $T(t, x, y, z)$ has to be obtained to correctly estimate the heat flux coming from the hot gas with a sufficient level of accurancy. Numerous attempts have been made in previous studies[7,9,10] to correlate in-wall temperature measurements to heat flux at the hot gas side. In the present paragraph, some of the developed tools and the achieved results are presented.

Determining the heat flux, knowning the temperatures in some of the points of the control volume basically implies the solution of an inverse problem. Inverse heat transfer problems are challenging due to their ill-posed nature as well as because surface conditions must be obtained from temperature sensors embedded within the objects, which experience attenuated and timelagged responses to changes in boundary conditions. Solution methods must therefore be stable and accurate in the presence of noisy signals. Most inverse methods are based on minimizing the sum of the square residual (J) of the difference between measurements and a solution of the heat flux equation. The same

procedure, as schematically presented in Fig. 3, is used for the present study. An initial estimate is made for the

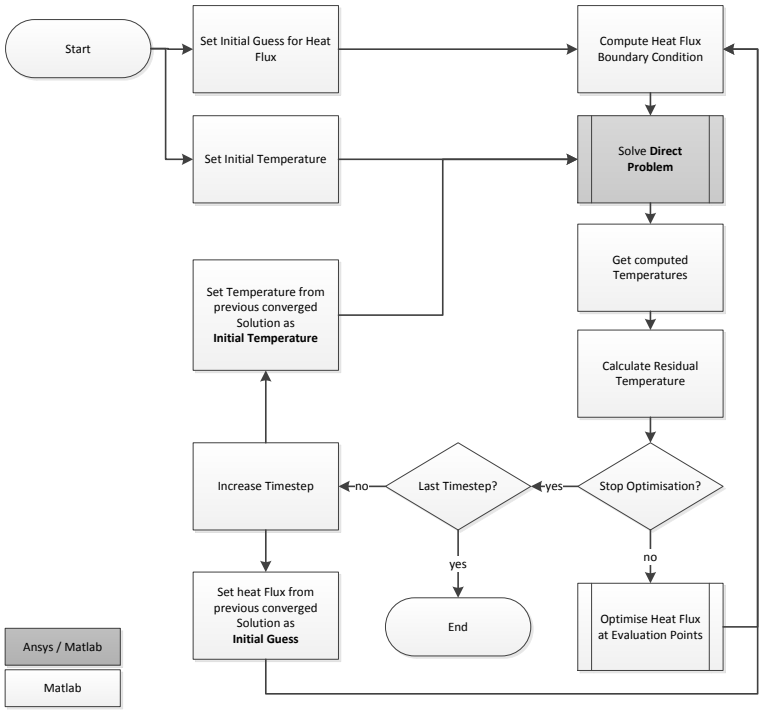

Figure 3: Iterative Process of an Inverse Method

boundary conditions, and a response at the sensor location is calculated. The calculation of the temperature in the desired position is addressed as solution of the direct problem. Then, the estimate is improved by means of the use of a disparate number of optimization techniques, until a convergence criterium for J is satisfied. The method used to calculate the response in the desired control volume is specific of the appproach chosen. Finite Elements (FEM) as well as Finite Difference (FDM) methods, both in 2D and 3D, are employed in the current work to solve the heat equation.

The complete evolution of the measured signals over time is considered when solving the inverse problem. The beginning of the unsteady heat-transfer phase to be evaluated is taken to be the time at which the chamber pressure reaches 90% of its stationary value, shown as t_{start} in Fig.2. The end time of the calculation is chosen to be at the end of the stationary combustion, shown as t_{end} in Fig.2.

While solving the inverse problem the following simplifications are done:

- Material properties are considered as constant since, for the range of temperature experienced in the combustion chamber, no significant variations are expected. The density ρ of OFHC copper is assumed to be constant as well as the thermal conductivity and the heat capacity.
- Uncertainities in thermcouples locations are negligible, since the sensors are installed in the high precisely drilled holes and kept in position by springs.
- No influence of the hot gas side is taken into account. Solely the heat conduction problem in the chamber material is solved and the input from the hot gas is taken to be constant along perimeter of the control volume boundary.

Finally, when comparing the obtained results, it is worth noticing that for a heat-sink chamber, the wall temperature increases. The heat flux changes accordingly with time. The local wall heat flux results therefore need to be considered along with the corresponding local wall temperatures. Furthermore, the slopes of both the wall temperatures and heat flux profiles versus time varies with the time into firing. In order to compare the results of different operating conditions on an even basis, it is advisable to average over the same interval across all targeted operating points. Clearly, better average values are obtained of these quantities if the averaging is conduced right before the end of the firing. Therefore, the average wall temperature and the heat flux results presented in this paper are obtained by averaging the results at the $2/3$ of the burning time over a $0.5\ s$ time interval. The data for the described time interval are further indicated as data evaluated at t_{eval}.

With the averaging procedure described as above, the results of the local wall temperature and heat flux versus axial location are shown for *CASE A* and *CASE B*.

3.1 "Quasi-steady state" 1D approach

Before proceeding to the solution of the inverse problem, with the goal to get a feeling of the heat flux for different operating conditions, as first step the attempt is made to obtain reliable results with a "quasi-steady state" 1D approach. The cumulative heat method is adopted by the observation of the time evolution of the temperature signal during the hot run. At the time interval t_{eval}, the temperature distribution is fully established and quasi-steady-state conditions can be assumed. Therefore, with the assumption of a constant heat flux, the temperature may be considered to equally change at any point of the combustion cross section, where the measurement sensor is installed. This allows defining the heat transfer problem only by the heat accumulated in the control volume itself. The observation of the temperature traces over time implies a constant slope $^{dT}/_{dt}$ at time t_{eval}, see Fig. 2. The measured temperature at 1 *mm* in the wall and its

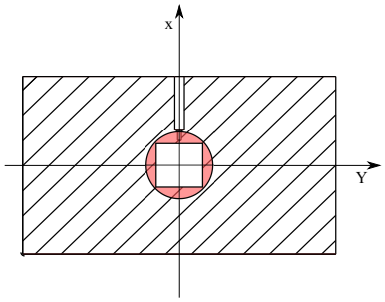

Figure 4: Control volume for the 1D heat flux calculations

variation over time is assumed as representative of the complete control volume and the geometry is approximate to a flat plate. The energy balance for the designed control volume is solved, since analytical solutions are in this case available for the heat transfer equation (Eq. 3).

$$\dot{E}_{in} - \dot{E}_{out} = \dot{E}_{stor} \tag{3}$$

Following this approach, previous studies[8,11] have made use only of the storage terms, reducing the control volume to a flat plate model. The variation of the temperature readings over time was directly linked to the heat flux on the combustion chamber walls. However, the obtained results have shown too high heat flux levels. This method suffers in fact of higher unceratines and tends to fail if the gradient of the temperature with the time becomes too strong, since it is assumed that the complete material is subject to the same variation of temperature over time as in the measurement position.

The strong variation in temperature (ca. 100 *K*) within the combustion chamber wall (x-direction/y-direction) and the distortions introduced by the additional material of the corners make the thermocouples signals evolution over time not representative for the whole cross section and lead to the mentioned overpredicitions. To infer the temperature distribution and the rate of heat flow through the system, the control volume has to be chosen in an appropiate way, such that the hypothesis for a 1D analysis can be more precisely met. Additionally, the distortions introduced from the geometry cannot be neglected and a simple flat plate model is not sufficient. Given these justifications, the method presented attempt to reduce the complexity of the temperature field to the determination of two parameters: r, the radius of the control volume, and X, the shape factor[12] characteristic of the geometry. Even if a shape factor is classically defined for multidimensional steady-state heat transfer problems, an accurate choice of the control volume allows for its use also in quasi-steady state conditions. The shape of the temperature isolines is only a function of the material properties and of the specific problems (geometry and boundary conditions) and they are independent from the heat flux level. Consequently, once the control volume has been chosen, X is constant even if the heat flux level changes. In order to identify the suited volume, the shape of the temperature field in the chamber cross section has to be inspected. A number of direct FEM analyses are performed for a 2D model of the combustion chamber cross section at increasing level of heat flux. Once the direct solutions are known, the temperature field is determined for every node of the simulated control volume. The process is then iterative and requires the minimization of three cost functions such to obtain the one in the desired control volume shown in Fig. 4. These functions are such that the following assumptions are met: the standard deviation of the measured temperature compared to the desired volume temperature, the variation of the heat flux on the boundaries of the chosen control volume and the difference of the incoming and outcoming heat

flux are as small as possible. The minimum of the combined function corresponds to the desired parameter r and the related values of X. The dimension of the so defined control volume is generally a function of the heat flux level, but it becomes equal to the minimum available radius, if the difference between the incoming and outcoming heat flux has to be as low as possible. The last requirement is fundamental in order to make a correct use of the shape factor. Once r and X are chosen the following balance equation Eq. 4 is valid for the outlined control volume:

$$\dot{q}_{in} - \dot{q}_{out} = \frac{mc\Delta T}{A_{hw}\Delta t} \tag{4}$$

The Eq. 4 is applied at each thermocouple position as it is independent of the temperature level. The properties, density, heat capacity and conductivity of the copper, are assumed constant. It is concluded that the rate of heat release to the inner walls due to combustion is equal to the rate of heat absorbed by the control volume, corrected by the heat loss due to conduction to the remaining material. In this way, transient temperature data are reduced to heat flux from an energy balance on a control volume containing the sensor. The temperature variation over time ($^{\Delta T}/_{\Delta t}$) is calculated from the measured temperature signals during the time interval t_{eval}. The heat loss is instead determined from Eq. 5:

$$\dot{q}_{out} = \frac{X}{A_{hw}}\lambda\left(T\left(t,1\right) - T\left(t,2\right)\right) \tag{5}$$

The temperatures at the boundaries $T(t,1)$ and $T(t,2)$ of the control volume, on the hot gas wall and at the radius r, are obtained from the measured temperatures, at the external surface of the combustion chamber wall and at 1 *mm* in the chamber walls. A linear temperature profile is assumed in the copper material. The results obtained with this method are shown for the *CASE A* and *CASE B* in Fig. 5. As shown in the figures, the level of heat flux is comparable between

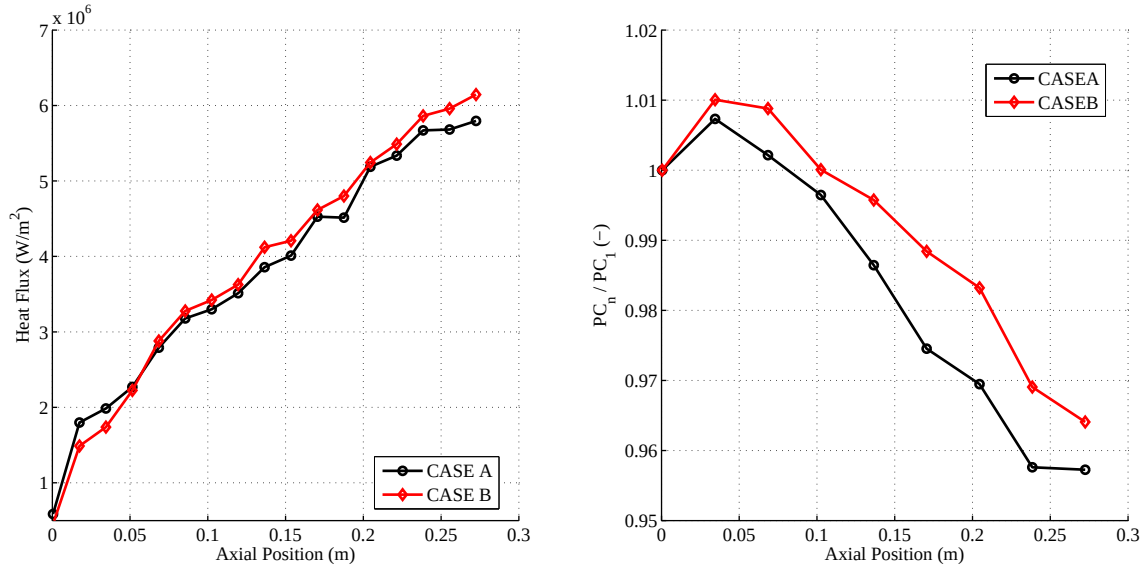

(a) (b)

Figure 5: Heat flux with 1D approach (a) and experimental normalized pressure (b) distribution along the chamber axis for *CASE A* and *CASE B*

the two load points. However, a difference in terms of flattening of the heat flux profile in the last part of the combustion chamber is visible . The lower mixture ratio (*CASE A*) shows a longer flat region towards the end of the combustion chamber. The plateau reached suggests the end of the combustion processes and this hypothesis is also confirmed by the pressure decay along the chamber wall.

3.2 2D FEM approach

The approach presented in the previous section, simplifies the complexity of the heat transfer problem in the combustion chamber wall to the determination of two characteristic parameters, which describe the distortion of the temperature field in the combustion chamber cross section. Such simplifications can anyhow be missleading, if not confirmed by

more refined analyses. For these reasons, an inverse heat transfer problem has to be solved and the unsteady heat conduction equation needs to be worked out to take into account transient effects. By increasing step-by-step the order of complexity, an inverse problem, which makes use of a 2D FEM analysis, is used to get the heat flux on the inner combustion chamber walls. The transverse cross section of the combustion chamber is chosen as computational domain in order to consider the cumulative effect of the copper material and the distortions caused by the presence of the corners. Due to the natural symmetry of the combustion chamber a reduced control volume is identified, which corresponds to a quarter of the combustion chamber as shown in Fig. 6. Each sensor is considered independent of

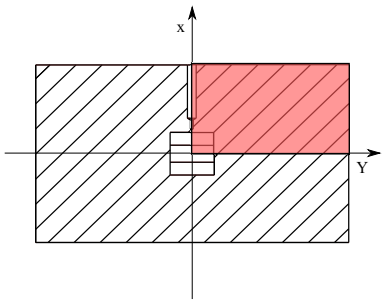

Figure 6: Control volume for the 2D FEM inverse problem

the others. The longitudinal heat flux due to conduction between the different measuring positions is neglected. Heat flux boundary conditions are imposed on the inner and the outer walls. The outer wall is assumed to be subject only to natural convection with a constant heat convection coefficient of $4\,W/(m^2K)$. The heat dissipated on the external boundaries (environment) is calculated for an extreme case considering air taken at ambient temperature ($288\,K$) and the outer wall temperature at $300\,K$, assuming forced convection with an air velocity of $15\,m/s$. This component of the heat flux can only account to 0.3% of the heat flux from the hot gas side. Therefore, it has to be expected that its influence is marginal. The internal surface heat transfer is evaluated differently depending on the hot run phase to get the right start-up and shut-down conditions. Three main phases are identified: pre-start-up, stable combustion and post-shut-down. During the pre-start-up, the heat flux coming from the hot gas is set to zero, whereas at the post-shut-down a new value of the heat flux is calculated to take into account the forced convection between the purging gas and the hot walls. During the stable combustion operation, the imposed heat flux is changed so that the temperatures obtained match the experimental results as close as possible. The heat flux imposed at the inner wall, for which the temperatures best approximate the measured values, is considered to be the optimum value. The discretized 2D heat transfer equation Eq. 6 is solved simultaneously, marching forward in time and applying the transient recessed thermocouple measurements.

$$\frac{\lambda}{(\partial x)^2}(T_{i+1,j,t} - 2T_{i,j,t} + T_{i-1,j,t}) + \frac{\lambda}{(\partial y)^2}(T_{i,j+1,t} - 2T_{i,j,t} + T_{i,j-1,t}) = \frac{\rho c}{(\partial t)}(T_{i,j,t+\partial t} - T_{i,j,t}) \tag{6}$$

A similar approach can be found in[13]-[14] for GOX/GH2. The evolution of the heat flux over time is approximate by a B-spline. The heat fluxes and the time constants in the heat flux evolution are adjusted in the iteration process, such that the experimental and the computed temperatures can be matched within 1 to $3\,K$. The following error function is implemented:

$$J = \frac{\left(\sum_j \sum_i w_j \left(T_{ij} - T_{M,ij}\right)^2\right)}{\sum_j w_j} \tag{7}$$

where i is the index for the axial positions and j for the discretized time intervals. The factor w_j is a function which weights the importance of the error over the evaluation interval. For the current study an equally distributed weight for the residual is chosen and w_j ist set equal to 1. Refering to the process scheme (Fig. 3), the optimazation step is an unconstrained nonlinear optimization which make use of the simplex search method of Lagarias et al. The function is used in order to minimize the error and get good approximated values of the thermocouples $T_i(x,t)$ positioned at $1\,mm$ in the wall for every time step dt. However differently from what reported in figure, the optimazation of the boundary conditions takes place after all timesteps have been run.

While performing the solution of an inverse problem, it can not be neglected that any thermocouple, which is at an initial temperature T_0, when used to measure an object that is at a constant temperature T has some response delay. Such delay has to be taken into account when evaluating the heat flux for a capacitive hardware. In the current study, the measured temperature continues to increase after the combustion starts, resulting in unsteady temperature and heat

flux at the wall. Because of the response delay of the thermocouples, there is some discrepancy between the real time temperature and the experimental output. The influence of this parameter has therefore to be investigated. Similar anaylsis can be found also in previous studies ([15]), where an attempt is made to reconstruct the real temperature signal from the value of τ.

In order to model the sensor response to an external excitation, it is assumed that the conduction within the thermocouple material is small compared to the heat transfer resistance between the material and the environment of the thermocouple, i.e. the copper material. Thus, the temperature gradient within the thermocouple is negligible. The transient temperature response can then be then determined by formulating an overall energy balance on the solid of the form in Eq.8:

$$\frac{dT_M}{dt} = \frac{T_M - T}{\tau} \tag{8}$$

The variable τ is the desired response time and it can be expressed as the product of a thermal resistance of the process at the interface and the lumped thermal capacity of the solid[12]: $\tau = R_t C_t$. Any change in R_t and C_t will cause a body to respond differently to any changes in its thermal environment. Due to the relative low computational costs of the approach presented in this paragraph, a similar mathematical model is implemented to attempt to determine the response time of the thermocouples installed in the combustion chamber walls. By proceeding independently for every thermocouple, the heat flux on the combustion chamber walls is linked to the response time of the sensors as presented in Eq. 8. The time-dependent boundary conditions are obtained by a proportionality to the combustion chamber pressure readings[16] through the constant C and the exponent n: $\dot{q}_{hg} = C\ P_c^n$. The exponent n is assumed equal to 0.8. A two parameters (τ, C) inverse problem on the cross section of the combustion chamber is than solved. The optimization of τ and C is possible within the same problem, since these two quantities are linearly independent from each other. The start-up phase and the shut-down phase are chosen as evaluation intervals, as in the transient of the combustion process the response influence in the signal comparison is maximal. Therefore τ can be determined with the maximum accurancy. The duration of evaluation time interval is chosen equal to 1 s in both cases. The process has to be reapeted for a large number of tests belonging to the same test campaign, during which the hardware is not dismounted and thermocouples are kept in position. The values obtained from the single tests are averaged over the total amount of tests available. Typical results are shown in Fig. 7 for the current test campaign. The plotted values are calculated as mean values between the two evaluation intervals and the complete set of tests available. A maximum standard deviation of about 10% is obtained. The variance is attributable to the difference between the values obtained at the start-up and at the shut-down evaluation phase. Changes in the duration of the evaluation time interval, used for

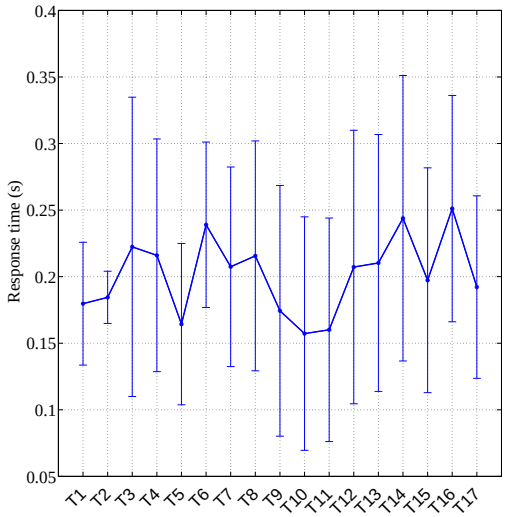

Figure 7: Response time for the present test campaign

the estimation of τ, have shown to have not a big impact on the values obtained. A deviation of less than the 1% has to be expected. Furthermore, the comparison with previous test campaigns, where the installed thermocouple set is the same and their installation was not varied, shows also only marginal deviations. The mean value for τ for the complete thermocouple set is of about 0.2 s.

The conversion of the temperature outputs to the heat flux with the 2D FEM analysis is then subdivided in 2 basic steps: first the determination of the relaxation time for the single thermocouple installed in the combustion chamber, then the solution of the inverse problem. The values calculated for τ are used to delay the temperatures predicted

from the FEM analysis according to Eq. 8, which have to match the measured ones to accept the inverse method as converged. Typical results obtained for one run of the code for the *CASE A* and *CASE B*, in terms of the heat flux and temperature, are shown in Fig. 8.

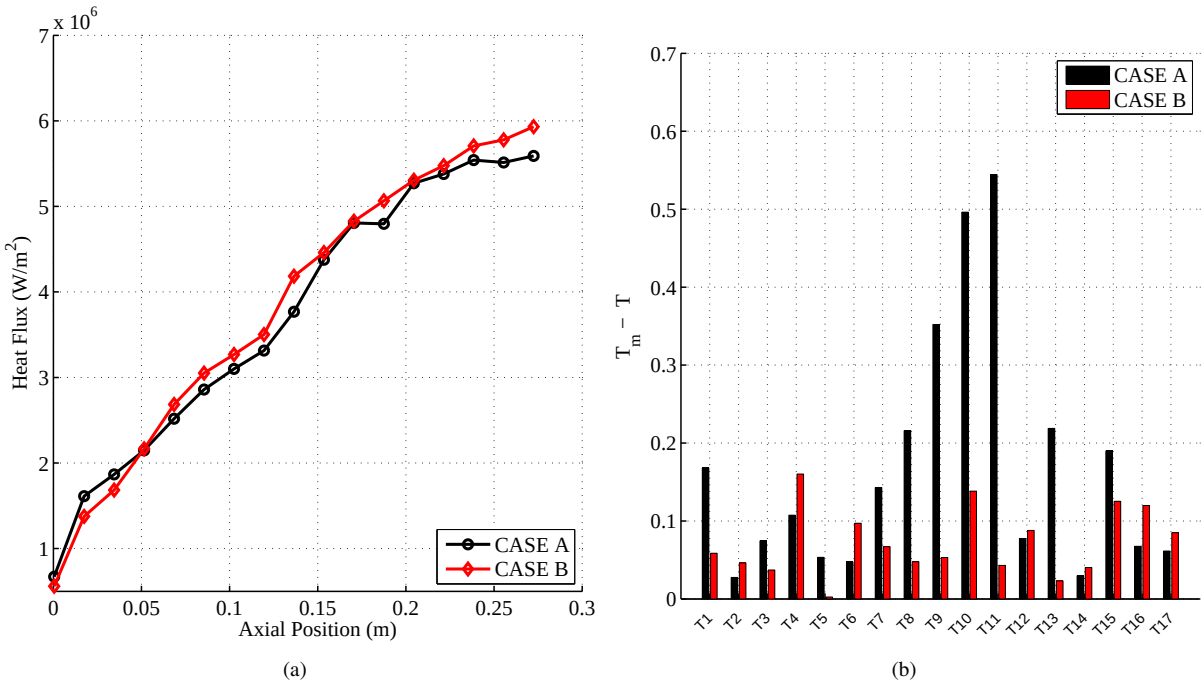

Figure 8: Heat flux distribution (a) and temperature error (b) along the chamber axis for *CASE A* and *CASE B* with 2D FEM approach

To get a feeling of the influence of the response time of the thermocouples, Fig. 9 shows the results obtained for the *CASE B* in terms of heat flux and temperature error along the chamber axis for different response time settings. The observation of a quite big standard deviation on the obtained results asks for such a sensitivity analysis. Runs of code for which τ is neglected are compared to ones obtained for τ beeing equal to 0.1 s for the complete thermocouple set, and to the ones resulting from calculated values of τ for the single thermocouples, as previously described. The results show that an influence is visible in the case the time response of the thermocouple is taken into account both on the error committed in predicting the measurement temperatures over time and on the heat flux along the combustion chamber walls. Variations of the value assigned to τ show instead to have only a marginal impact and no significant differences can be highlighted. To conclude, it can be seen that even though the difference between the time constants is of about 50%, the calculated temperatures differ by less than 0.5 K, which is an acceptable deviation considering the total temperature increase of ca. 100 K. Further accurancy improvement is limited by the accuracy of the sensors iteself ($\pm 5K$).

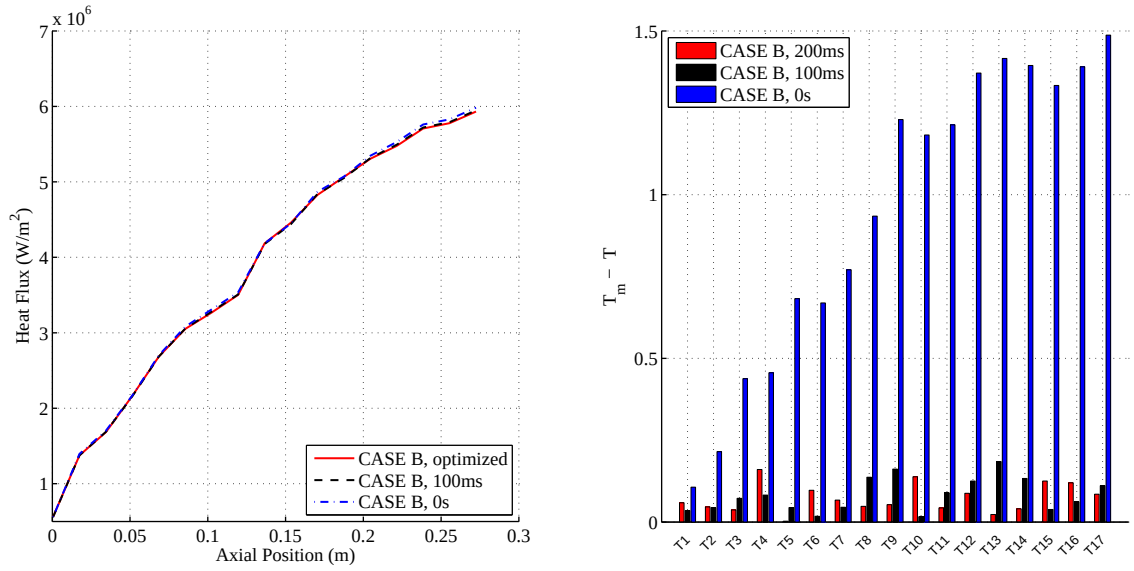

(a) (b)

Figure 9: Heat flux along the chamber axis (a) and temperature error (b) for *CAS E B* with different set values of τ

3.3 3D Finite Difference based Inverse Regularization Method

The present method is based on a Finite Difference (FD) scheme which is applied on the discretized 3D domain of the combustion chamber. The optimization method for the solution of the inverse problem relies on an iterative method and specifically on the Inverse Regularization Method (IRM).[17] The resulting heat flux is determined solely by the thermocouple measurements and the conduction properties of the chamber. The computational domain is simplified and restricted to the combustion chamber, starting from the faceplate and ending at the axial position where the nozzle begins. The nozzle itself is not included, since no sensors are attached in this engine segment and therefore, no information about its temperature can be obtained. The boundary condition at the surfaces being in contact with the atmosphere is described by natural convection. At the faceplate, a conductive boundary condition is implemented. This is achieved by modeling an extra copper block of $0.029\,m$ in length, which acts as a heat sink, as seen in Fig. 1. The boundary conditions for the plane in contact with the nozzle is defined as adiabatic. A sensitivity analysis with von Neuman boundary conditions which took into account the axial heat transfer from the nozzle, were carried out. The results showed however no significant variations compared to the adiabatic case. A schematic description of the inverse method is illustrated in Fig. 3. At first, the temperature initialization takes place with the information provided by the thermocouples at the starting time. The optimization variable, namely the heat flux, is initialized with a default initial guess. By applying this heat flux as the boundary condition of the hot gas wall for the duration of a computational time step dt, the temperature distribution over the whole domain is obtained. Upon comparison of the measured and computed temperatures for the M thermocouple positions, the residual function is defined as:

$$J = \sum_{n=1}^{M} \int_0^t (T_{FD}(\vec{x}_n, t) - T_M(\vec{x}_n, t))^2 \mathrm{d}t \tag{9}$$

J is also the cost function which has to be minimized. In case this value has converged below the targeted limit, the optimization process is stopped for this time step, otherwise the regularization method takes over. The IRM is based on the formulation of the initial and boundary conditions as necessary optimality conditions by utilizing the Lagrange multipliers g_i. This leads to the Lagrange functional L:

$$L = \sum_{n=1}^{M} \int_0^t (T_{FD}(\vec{x}_n, t) - T_M(\vec{x}_n, t))^2 \mathrm{d}t + \int_0^t \oint_V g_V(\vec{x}, t)\left(\nabla^2 T(\vec{x}, t) - \frac{1}{a}\frac{\partial T}{\partial t}\right)\mathrm{d}V\mathrm{d}t + \oint_V g_0(\vec{x})(T_{FD}(\vec{x}, 0) - T_0(\vec{x}))\mathrm{d}V + \sum_{i=1}^{4} \int_0^t \oint_{S_i} g_i(\vec{x}, t)\left(u_i(\vec{x}, t) + \lambda\frac{\partial T}{\partial \vec{n_i}}\right)\mathrm{d}S_i\mathrm{d}t \tag{10}$$

a is the thermal diffusivity $a = \frac{\lambda}{\rho c_p}$, a material constant depending on the heat conductivity λ, the density ρ and the specific heat capacity c_p and $T_o(\vec{x})$ stands for the initial temperature along the domain of the chamber. Since the initial temperature $T_o(\vec{x})$ is not necessarily uniform throughout the chamber but is known only at the discrete positions of the thermocouples, certain interpolation and extrapolation methods are utilized in order to obtain the initial temperature distribution over the full domain. This way the third term of the lagrange function is satisfied, by the proper initialization of the computed temperature at $t = 0$. The last term in Eq. 10 represents the four boundary conditions (combustion chamber hot gas wall, contact to atmosphere, nozzle and faceplate). The term $\frac{\partial T}{\partial \vec{n_i}}$ represents the partial derivatives along the boundary normals. The boundary condition at the hot gas wall $u_1(\vec{x}, t)$, represents the unknown heat flux $\dot{q}(\vec{x}, t)$ and is the variable to be optimized. The value of $\dot{q}(\vec{x}, t)$ is a function of the axial length and of time, remains however constant along the circumference of the hot gas wall.

The necessary optimality condition for the Lagrange functional is that its variation reaches zero for a small variation of $\dot{q}(\vec{x}, t)$, as described in Eq. 11.

$$\delta L\,(\dot{q}(\vec{x}, t), \delta\dot{q}(\vec{x}, t)) = 0 \tag{11}$$

The formulation of the Lagrange variation leads to the calculation of the three last Lagrange multipliers (g_2, g_3, g_4) and to the defition of a new set of PDEs for $g_1(\vec{x}, t)$. This set of equations and boundary conditions builds the adjoint problem.[17]

$$\frac{1}{a}\frac{\partial g_1(\vec{x}, t)}{\partial t} = -\nabla^2 g_1(\vec{x}, t) - 2\sum_{n=1}^{M}(T_{FD,n}(t) - T_{meas,n}(t))\delta(\vec{x}, \vec{x_n}) \tag{12}$$

The corresponding boundary conditions take the form:

$$\lambda\frac{\partial g_1(\vec{x}, t)}{\partial \vec{n_i}} = -u_i(\vec{x}, t) \tag{13}$$

The adjoint problem has the same form as the direct heat conduction problem and can therefore be solved with the same direct solver along the domain. According to Artioukhine,[17] the gradient of the residual function, $\grave{J}$, is given by:

$$\grave{J}(\vec{x}, t, \dot{q}) = \frac{1}{\lambda} g_1(\vec{x}, t) \tag{14}$$

Since the gradient of the residual function is known, a minimization algorithm can be used to obtain the sought optimum. The chosen algorithm is the conjugate gradient method, which requires two parameters for the update of the optimization variable. The first parameter, namely the descent direction $\delta\dot{q}$, is obtained directly from $\grave{J}$.[18] The influence of this heat flux variation on the temperature variation $\theta = (T - T_0)$, has to be calculated in the domain. This is achieved with the solution of the direct problem in variation.

$$\frac{1}{a}\frac{\partial\theta(\vec{x}, t)}{\partial t} = -\nabla^2\theta(\vec{x}, t) \tag{15}$$

With the updated conditions for the boundaries:

$$\lambda\frac{\partial\theta(\vec{x}, t)}{\partial \vec{n_1}} = -\delta\dot{q}(\vec{x}, t) \quad \text{and} \quad \lambda\frac{\partial\theta(\vec{x}, t)}{\partial \vec{n}_{2,3,4}} = 0 \tag{16}$$

The final step after the solution of $\theta(\vec{x}, t)$ is found, is the calculation of the second descent parameter γ for the updated heat flux. This is a function of the temperature variation θ.[18] The updated heat flux at iteration step $k + 1$ is then given by:

$$\dot{q}_{k+1}(\vec{x}, t) = \dot{q}_k(\vec{x}, t) + \gamma\,\delta\dot{q}(\vec{x}, t) \tag{17}$$

The new heat flux is applied to the boundary and the procedure is repeated for each time step until convergence.

An important advantage of the code is the fact that the solution of each direct problem is performed on a simplified geometry, for which the code has been optimized. This way, the solution of the direct problem is faster for this specific rectangular block geometry than in the case of commercial solvers. Therefore, the fact that 3 different direct problems have to be solved during each iteration (direct solution, adjoint problem and direct problem in variation) is not so evident in the computational time. However, the code is limited only to the predefined combustion chamber geometry and is not flexible in case of a geometry change (for example a change in shape from rectangular to cylindrical). The results for two test cases are presented in this section with load points at 2 MPa $ROF = 2.2$ and 2 MPa, $ROF = 3.4$ respectively. The heat flux and temperature profiles over axial length are depicted in Fig. 10, whereas the time profiles of the temperature at two thermocouple positions are illustrated in Fig. 11. Good agreement between the measured signal and the calculated value is observable during the complete test for both operating points.

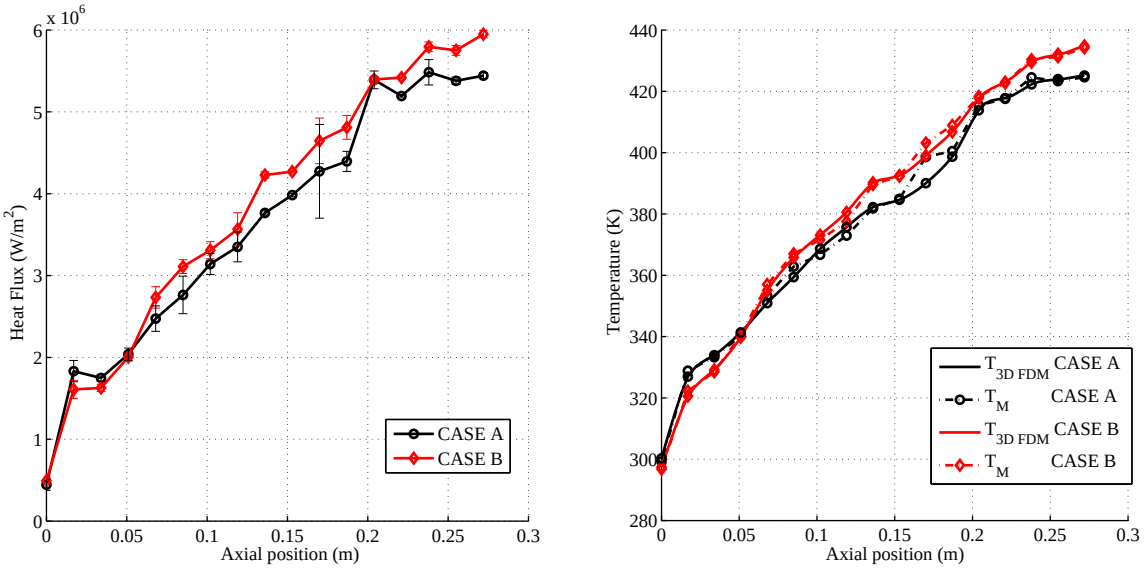

(a) (b)

Figure 10: Heat flux (a) and temperature results (b) over axial positions for Case A and Case B obtained with 3D FDM

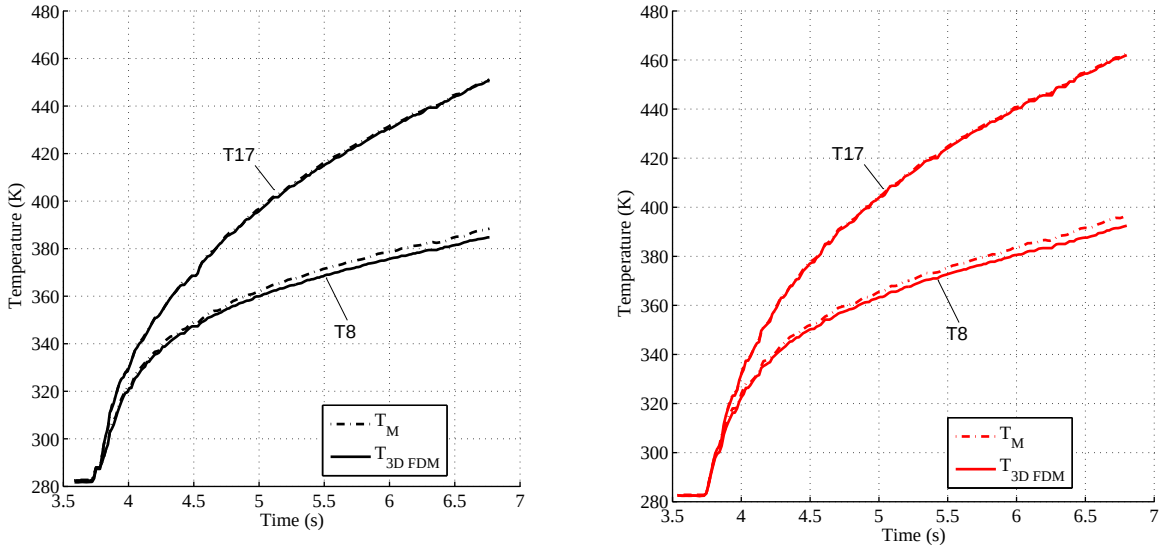

Figure 11: Temperature profile along time for Case A (a) and Case B (b) for 3D FDM

3.4 3D FEM-Based IHCP Method

The present method makes use of and combines commercially available off-the-shelf engineering tools to solve the inverse heat conduction problem (IHCP) for rocket combustion chambers. The aim is to obtain the heat flux, which is originating from the combustion and is subject to the hot gas walls of the combustion chamber. This is achieved by iteratively calculating temperature distributions in the combustion chamber walls for varying heat flux values and comparing the resulting temperatures to experimental measurement data.[19] The solution of the temperature distributions, also called the direct problem, is done with a finite element approach.

The variation of the heat flux is based on a conjugate gradient optimization method.[20] In order to reduce the time needed of the optimization of the heat flux values, the heat flux is only optimized at discrete points. The heat flux boundary condition of the direct problem is calculated from the optimized heat flux values with the help of interpolation methods. The points for which the heat flux is optimized are called parameters.

This heat flux optimization is performed separately for each time step. The time steps are linked by the forced continuity of the heat flux and the temperature distributions over time.

The flowchart in figure 3 shows the sub steps of this procedure. Starting with an initial temperature distribution and an arbitrary set of parameters, the direct solution of the temperature field is computed. The resulting temperatures are then compared to the measured temperatures. If the stopping criterion is not met, the parameters are varied according to the conjugate gradient method and the direct solution is calculated again in order to minimize the residual value J, which is based on the measured temperatures $\boldsymbol{Y}$ and the computed temperatures $\boldsymbol{T}$ in dependence of the iterated heat flux parameters $\boldsymbol{P}$ at iteration k .

$$J(\boldsymbol{P}) = \left[\boldsymbol{Y} - \boldsymbol{T}\left(\boldsymbol{P}^k\right)\right]^T \left[\boldsymbol{Y} - \boldsymbol{T}\left(\boldsymbol{P}^k\right)\right] \tag{18}$$

The decision which parameters are varied by which magnitude in order to reduce the overall temperature error is based on the sensitivity principle. Therefore, the sensitivity of temperature changes at each sensor with respect to parameter deviation at all parameter locations is assessed in advance to the inverse solution itself. The result is the Jacobi matrix in Eq. 19.

$$\mathbf{S}^k = \begin{bmatrix} \frac{\partial T_1}{\partial P_1} & \cdots & \frac{\partial T_M}{\partial P_1} \\ \vdots & \ddots & \vdots \\ \frac{\partial T_1}{\partial P_N} & \cdots & \frac{\partial T_M}{\partial P_N} \end{bmatrix}^k \tag{19}$$

The stopping criterion, as given in Eq. 20, is based on the measurement error of the temperature readings, where

σ denotes the standard variation of the temperature readings at a constant temperature. This value accommodates the measurement noise. The additional summand ψ accommodates errors inherent to the used thermocouples themselves, e.g. temperature off-sets, as well as errors caused by the positioning of the sensors.

$$J \leq \sum_{i=1}^{I} \sigma^2 + \psi \tag{20}$$

In case that the stopping criterion for the current time step is met, the computation of the next time step is triggered. Therefore, the heat flux distribution from the preceding time step is used as initial parameter guess together with the corresponding temperature distribution.

The heat flux profile needs to be continuous to obtain a physically reasonable heat flux profile as outcome of the optimization. In order to assure the continuity of the heat flux in spatial dimension, the heat flux profile is smoothened around steps and non-continuous singularities with the help of shape-preserving spline fitting algorithms.

The main algorithms, including the conjugate gradient based optimizer, are developed for MATLAB from The MathWorks, Inc. The direct finite element solution is implemented in ANSYS. Nevertheless, the interface is file based and allows for the use of different solution tools.

The plots in Fig. 14 show the heat flux profiles yielded with the presented method along the combustion chamber axis. The heat flux is assumed to be constant over the circumference of the hot gas wall. All results presented in this section are computed with temperature data acquired in a distance of 1.0 *mm* from the hot gas wall. The direct solution is computed without nozzle influence for every iteration. It is noteworthy that in Fig. 13, the measured temperature evolution at the two axial positions during the whole burning time is well reproduced by the calculated values. Fig. 14 shows instead for the two analysed cases the heat flux variation which looks different in the first and in the second segment where the heat flux tends to increase during the burning time.

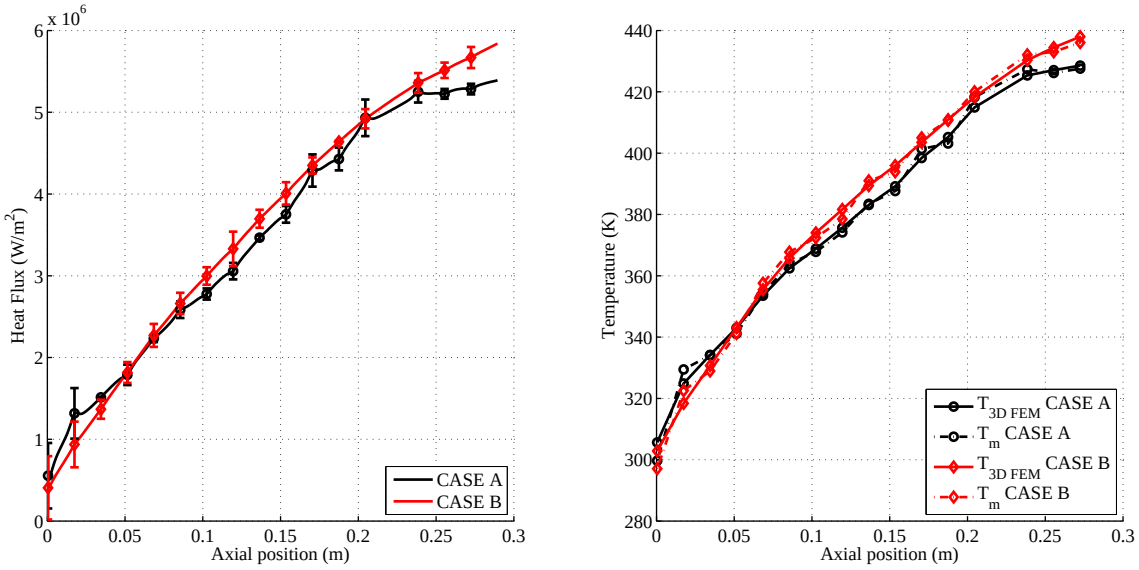

(a) (b)

Figure 12: Heat flux (a) and temperature (b) distribution along the chamber axis for *CASE A* and *CASE B* with the 3D FEM

4. Comparison

Results obtained with the 2D FEM, the 3D FEM as well as the FDM are compared at the evaluation time, when the experimental conditions reached complete stable operation. The heat fluxes determined along the axial direction are shown in Fig.15 for the operating *CASE A* and *CASE B*. The outcomes of the different approaches presented show a good agreement for both load points. The general trend and shape of the thermal loads on the combustion chamber walls, resulting from the flame interaction, is comparable. The difference in the flattening of the heat flux profile is shown by all methods, which proves the sensitivity of the codes to hot gas condition variations. The results

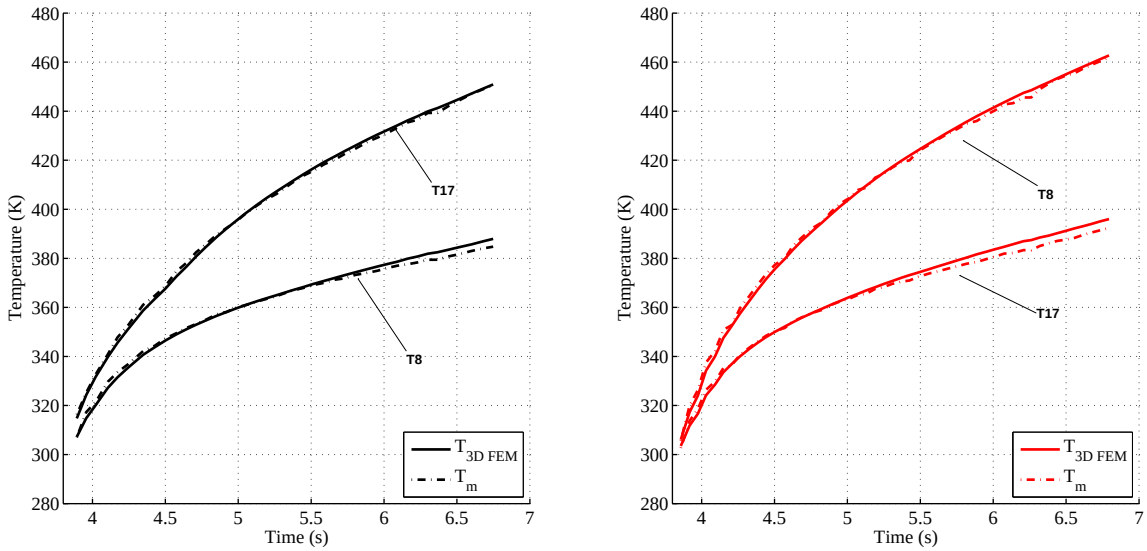

Figure 13: Computed and measured temperature distribution for *CASE A* (a) and *CASE B* (b) with the 3D FEM

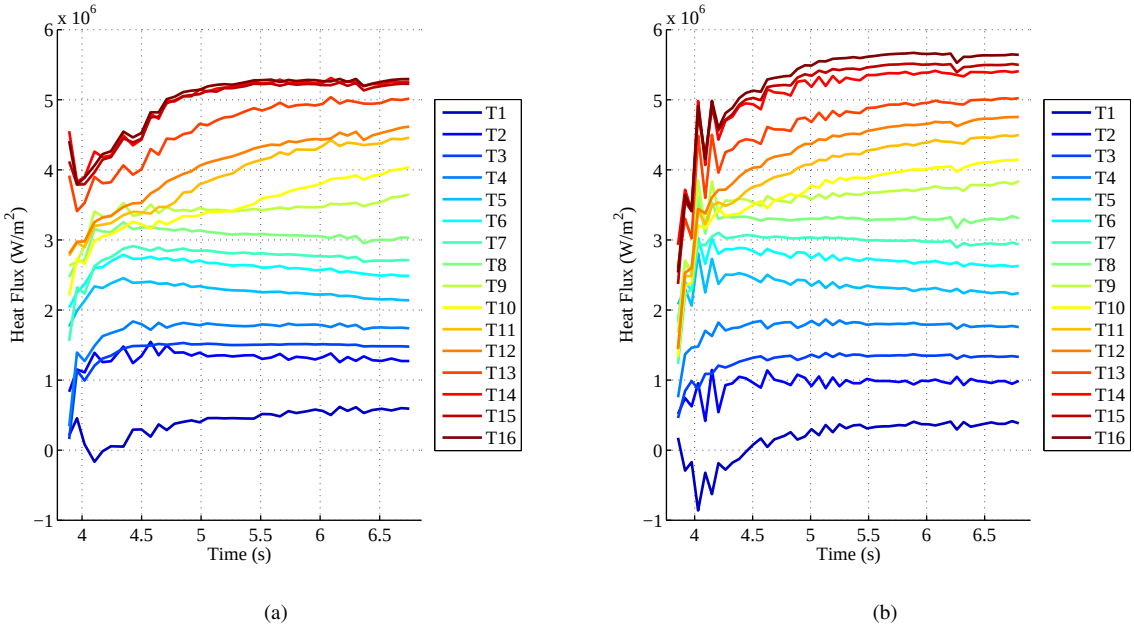

Figure 14: Heat flux over time at different temperature sensor positions for *CASE A* (a) and *CASE B* (b) with the 3D FEM

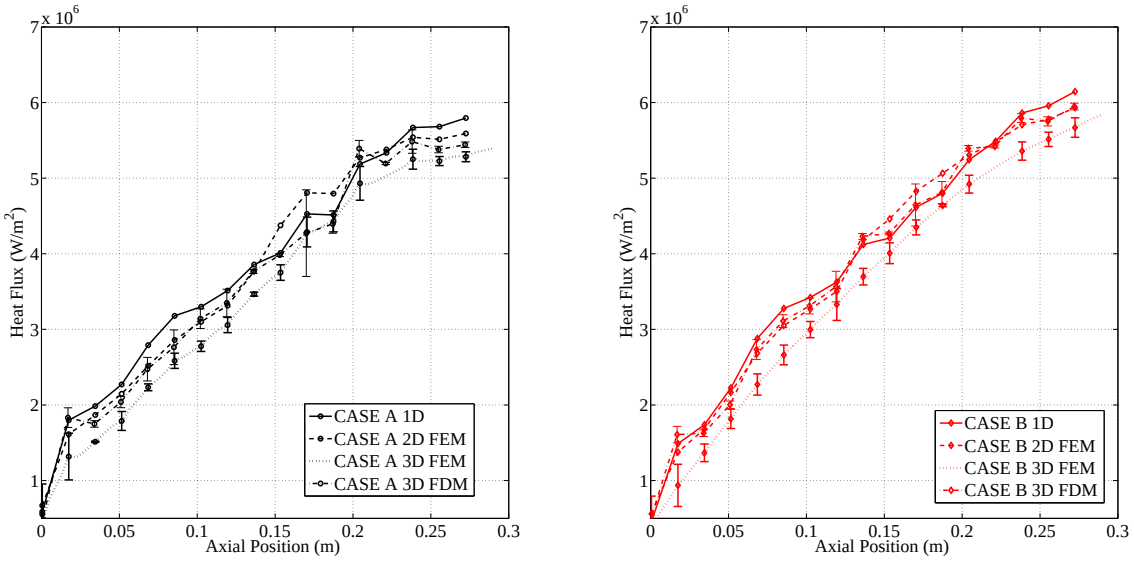

(a) (b)

Figure 15: Heat flux results comparison a) *CASE A* b) *CASE B*

obtained with a 2D model show, as expected, higher values for the heat flux, due to the neglected transversal heat flux. Differences between the two 3D approaches are for almost all the axial positions in the range of accurancy of the codes.

In order to judge the quality of the solutions obtained from the two 3D calculation methods, the heat flux is shown together with the temperature error e_T at the different axial positon positions. The temperature error e_T is given by Eq. 21.

$$e_T = \frac{T_{FEM} - T_M}{T_M} \tag{21}$$

The percentual error obtained is reported only for the axial position where its maximum value is reached. Furthermore, the heat rate at $t = t_{eval}$ is obtained by integrating the calculated heat flux over the surface of the combustion chamber. The results are summed up in Table 3.

Table 3: Inverse Heat Flux Results

Case	*CASE A*		*CASE B*	
	3D FEM	3D FDM	3D FEM	3D FDM
max. $\dot{q}$ in $[W/m^2]$	5.392	5.484	5.840	5.948
max. e_T in [%]	2.000	2.180	1.530	2.042
Accumulated Heat in $[W]$	48970	51895	50602	55301

Even if the error committed on the temperature predictions is of the same order of magnitude, the calculated accumulated heat by the 3D FEM is ca. 10% lower than the one obtained with the 3D FDM. The difference in the peak values is however not bigger than the 3%.

Both calculations based on 3D computations and assumption a 1D “quasi-steady state” approach show the same qualitative trend but the heat flux determined from the latter is relatively higher. The peak value of heat flux determined from the 1D heat calculations is 12% higher then the one calculated with a 3D FEM approach.

5. Conclusion

This study generates a comprehensive database of wall heat fluxes for a GCH4/GOX combustion at an ROF of 2.2 and 3.4 for a combustion pressure of 2 MPa. The comparison between the heat fluxes calculated from 1D, 2D and 3D analysis shows that the predicted peak values are varying in the range of 15%. The assumption of negligible heat tranversal heat conduction in the material can therefore lead to errors in the heat flux calculation in this order of magnitude. Hence, the use of a 3D approach is recommended for more detailed studies.

However, results obtained from the 1D model are able to predict the general trend of the heat flux evolution along the combustion chamber. Even if simplifications have been applied to solve the transient heat conduction problem, the main phenonema controlling the heat transfer in the copper material are represented. Due to the simple use of the method and the limited computational effort needed, such an appproach is recommended to get a good first estimation of the level of thermal loads in the combustion chamber.

6. Acknowledgments

Financial support has been provided by German Research Foundation (Deutsche Forschungsgemeinschaft-DFG) in the framework of the Sonderforschungsbereich Transergio 40.

References

[1] F. Cuoco, B. Yang, and M. Oschwald, editors. *Experimental Investigation of LOx/H2 and LOx/CH4 Sprays and Flames*, 2004.

[2] J. Lux, D. Suslov, M. Bechle, M. Oschwald, and O.J. Haidn. Investigation of Sub- and Supercritical LOX/Methane Injection using Optical Diagnostics. *AIAA 2006-5077*.

[3] T. E. Diller. Advances in Heat Flux Measurement. *Advances in Heat Transfer*, 23:279–368.

[4] A. Conley, A. Vaidyanathan, and C. Segal. Heat Flux Measurements for a GO2/GH2 Single-Element, Shear Injector. *Journal of Spacecraft and Rockets*, 44(3):633–639, 2007.

[5] G. Jones, C. Protz, B. Bullard, and J. Hulka. Local Heat Flux Measurements with Single Element Coaxial Injectors. *AIAA 2006-5194*.

[6] W. Marshall, S. Pal, R. Woodward, and R. Santoro. Benchmark Wall Heat Flux Data for a GO2/GH2 Single Element Combustor. *AIAA 2005-3572*.

[7] A. Vaidyanathan, J. Gustavsson, and C. Segal. One- and Three-Dimensional Wall Heat Flux Calculations in a O2/H2 System. *Journal of Propulsion and Power*, 26(1):186–189, 2010.

[8] M.P. Celano, S. Silvestri, G. Schlieben, C. Kirchberger, and O.J. Haidn. Injector Characterization for a GOX-GCH4 Single Element Combustion Chamber. 5^{th} *European Conference For Aeronautics And Space Sciences (EUCASS)*, 2013.

[9] Edward B. Coy. Measurement of Transient Heat Flux and Surface Temperature Using Embedded Temperature Sensors. *Journal of Thermophysics and Heat Transfer*, 24(1):77–84, 2010.

[10] G. Cai , X. Wang , and T. Chen . Method for Measurement of Single Injector Heat Transfer Charateristics and its Application in Studying Gas-Gas Injector Combustion Chamber.

[11] M.P. Celano, S. Silvestri, G. Schlieben, C. Kirchberger, and O.J. Haidn. Experimental and Numerical Investigation for a GOX-GCH4 Single Element Combustion Chamber. 4^{th} *Space Propulsion, 2014*, 2013.

[12] Incropera, DeWitt, Bergmann, and Lavine. *Fundamentals of Heat and Mass Transfer.*

[13] A. Vaidyanathan, J. Gustavsson, and C. Segal. Heat Fluxes/OH PLIF Measurements in a GO2-GH2 Single-Element, Shear Injector. *AIAA 2007-5591*.

[14] J.M. Locke, S. Pal, and R.D. Woodward. Chamber Wall Heat Flux Measurements for a LOX/CH4 Propellant Uni-Element Rocket. *AIAA 2007-5547*.

[15] X. Wang, Y. Gao, G. Cai , and H. Huo . Wall Heat Transfer Measurements in High-Pressure Combustion Devices. *J. Aerosp. Eng.*, 26:698–707.

[16] D.R Bartz. A simple Equation for Rapid Estimation of Rocket Nozzlle Convective Heat Transfer Coefficients. *Journal of Jet Propulsion*, pages 49–51, Jan. 1957.

[17] E. Artioukhine. Heat transfer and inverse analysis. *RTO-EN-AVT-117*, 2005.

[18] H. Cheng-Hung and C. Wei-Chung. A three-dimensional inverse forced convection problem in estimating surface heat flux by conjugate gradient method. *International Journal of Heat and Mass Transfer*, 43:3171–3181, 2000.

[19] D. Kuhl, A. Holzer, and O.J. Haidn. Computational solution of the inverse heat conduction problem of rocket combustion chambers. *AIAA99-2913*.

[20] M.N. Özisik and H.R.B. Orlande. *Inverse Heat Transfer - Fundamentals and Applications*. Taylor & Francis, New York, 2000.